

# The global 21 centimeter background from high redshifts

Steven R. Furlanetto\*

*Yale Center for Astronomy and Astrophysics, Yale University, 260 Whitney Avenue, New Haven, CT 06520-8121*

31 October 2018

## ABSTRACT

We consider the evolution of the sky-averaged 21 cm background during the early phases of structure formation. Using simple analytic models, we calculate the thermal and ionization histories, assuming that stellar photons dominate the radiation background. The resulting 21 cm spectra can constrain the properties of the first generations of stars and quasars. If Population II stars dominate, Ly $\alpha$  coupling renders the IGM visible before it is heated by X-rays and long before reionization. Thus the 21 cm background has a strong absorption epoch followed by weaker emission that fades during reionization. The harder spectra of very massive Population III stars compress these transitions into a shorter time interval and decreases the signal amplitude. However, the reionization epoch will remain visible except in extreme cases. The global 21 cm signal will be challenging to observe because of astronomical foregrounds, but it offers an exciting opportunity to study the first sources of light. It also fixes the overall amplitude of the fluctuating background whose detection is a major goal of several next-generation low-frequency radio interferometers.

**Key words:** cosmology: theory – intergalactic medium – diffuse radiation

## 1 INTRODUCTION

The earliest generations of cosmic structures have profound effects on the Universe around them and on later generations of stars and galaxies. These sources “reionize” the intergalactic medium (IGM), enrich galaxies (and the IGM) with the first heavy elements, and seed larger galaxies.

Observations now paint a fascinating – but confusing – picture of their properties. Unfortunately, observing “typical” galaxies at  $z \gtrsim 8$  is beyond the capabilities of existing instruments (though see Bouwens et al. 2004), so current constraints use reionization as an indirect proxy. The rapid evolution of the mean Ly $\alpha$  optical depth in quasar absorption spectra seems to indicate that reionization is ending at  $z \sim 6$  (Fan et al. 2001, 2005). Corroborating evidence comes from the proximity zones around these quasars, which also imply rapid evolution in the mean ionized fraction  $\bar{x}_i$  (Wyithe & Loeb 2004; Mesinger & Haiman 2004; Wyithe et al. 2005; Fan et al. 2005), as well as large-scale fluctuations in the transmission. But both are difficult to interpret: the latter, for example, may also be characteristic of reionization (Wyithe & Loeb 2005; Fan et al. 2005), but so far the variations are also consistent with density fluctuations (Lidz et al. 2006). On the other hand, large-scale polarization of the cosmic microwave background (CMB) observed by *WMAP* implies an early beginning to reionization at  $z \gtrsim 10$ , albeit with large uncertainties (Page et al. 2006; Spergel et al. 2006). How these puzzle pieces fit together – and, more fundamentally, how luminous sources

evolve, how feedback processes (such as metal enrichment, photoionization, or other radiation backgrounds) influence them, and how small-scale structure evolves in the IGM – remain mysterious (Wyithe & Loeb 2003a; Cen 2003b; Wyithe & Loeb 2003b; Cen 2003a; Haiman & Holder 2003; Somerville & Livio 2003; Fukugita & Kawasaki 2003; Onken & Miralda-Escudé 2004; Furlanetto & Loeb 2005; Choudhury & Ferrara 2005; Iliev et al. 2005). Unfortunately, identifying the relevant feedback processes and uncovering the source properties are impossible with existing data.

One promising method to disentangle these degeneracies is the 21 cm transition of neutral hydrogen (see Furlanetto et al. 2006 for a review). Before reionization, the neutral IGM gas should be visible against the CMB through this transition (Field 1958; Sunyaev & Zeldovich 1972; Hogan & Rees 1979). In principle, we can use it to map out the growth of the cosmic web and HII regions at  $z \gtrsim 6$  (Scott & Rees 1990; Madau et al. 1997; Zaldarriaga et al. 2004). The key advantage of the 21 cm transition is that it is a line: hence every observed frequency corresponds to a different distance, and we can isolate each phase in the IGM’s history.

Of the many applications of the 21 cm line, the simplest (at least conceptually) is to measure the global background as a function of frequency. This would allow us to measure  $\bar{x}_i(z)$  and, at earlier redshifts, the growth of soft-ultraviolet (UV) and X-ray radiation backgrounds, which are difficult to constrain in any other way. Three quantities are relevant: the thermal history, the Ly $\alpha$  background (both of which determine the spin temperature  $T_S$  of the IGM), and the ionization history (which determines when the signal fades). Unfortunately, this global background is likely to be diffi-

\* Email: sfurlane@tapir.caltech.edu

cult to measure because of contamination by Galactic synchrotron radiation (see §8). As a result, it has received little theoretical attention, and most existing work has simply argued that  $T_S \gg T_\gamma$  (where  $T_\gamma$  is the CMB temperature) during reionization (e.g., Madau et al. 1997; Ciardi & Madau 2003; Chen & Miralda-Escudé 2004). This is unfortunate because a number of efforts are nevertheless underway to observe it (and the challenges are not necessarily much greater than observing fluctuations in the background). Indirect techniques may also allow us to measure the background (Barkana & Loeb 2005b; Cooray 2005). And, of course, the global signal sets the overall amplitude of fluctuations, so those should be considered within this context. One exception is Sethi (2005), who studied the evolution of the global background in a limited set of models that did not fully explore the many uncertainties in the properties of the first sources.

The purpose of this work is to compute the high-redshift 21 cm signal and to identify those properties that can be measured from the mean background. Because we know so little about the first sources, it is of course impossible to make robust predictions for the background. We will instead parameterize the relevant processes and consider how they affect the mean signal. We first give some background on the 21 cm transition in §2. We then describe processes relevant to the thermal history of the IGM in §3, to the spin temperature in §4, and to the ionization history in §5. We then describe some general consequences for the 21 cm history in §6 and examine some specific models in §7. We conclude in §8.

In our numerical calculations, we assume a cosmology with  $\Omega_m = 0.26$ ,  $\Omega_\Lambda = 0.74$ ,  $\Omega_b = 0.044$ ,  $H = 100h \text{ km s}^{-1} \text{ Mpc}^{-1}$  (with  $h = 0.74$ ),  $n = 0.95$ , and  $\sigma_8 = 0.8$ , consistent with the most recent measurements (Spergel et al. 2006), although we have increased  $\sigma_8$  from the best-fit *WMAP* value in order to improve agreement with weak-lensing data.

## 2 THE 21 CM TRANSITION

We review the relevant characteristics of the 21 cm transition here; we refer the interested reader to Furlanetto et al. (2006) for a more comprehensive discussion. The 21 cm brightness temperature (relative to the CMB) of a patch of the IGM is

$$\delta T_b = 27 x_{\text{HI}} (1 + \delta) \left( \frac{\Omega_b h^2}{0.023} \right) \left( \frac{0.15}{\Omega_m h^2} \frac{1+z}{10} \right)^{1/2} \times \left( \frac{T_S - T_\gamma}{T_S} \right) \text{ mK}, \quad (1)$$

where  $\delta$  is the fractional overdensity,  $x_{\text{HI}} = 1 - x_i$  is the neutral fraction, and  $x_i$  is the ionized fraction. Note that the patch will appear in absorption if  $T_S < T_\gamma$  and emission otherwise. Here we have assumed that the patch expands uniformly with the Hubble flow; radial peculiar velocities also affect  $\delta T_b$  by changing the mapping from distance to frequency (Bharadwaj & Ali 2004; Barkana & Loeb 2005a). However, these anisotropic fluctuations do not affect the mean signal, so we will ignore them. We will use  $\bar{x}_i$  to denote the globally averaged ionized fraction; the temperatures are likely to be much more uniform at most times, and we will implicitly treat them as independent of position (though see Barkana & Loeb 2005b).

The spin temperature  $T_S$  is determined by competition between three processes: scattering of CMB photons, collisions, and scattering of Ly $\alpha$  photons (Wouthuysen 1952; Field 1958). In equilibrium (Hirata 2005),

$$T_S^{-1} = \frac{T_\gamma^{-1} + \bar{x}_\alpha \tilde{T}_c^{-1} + x_c T_K^{-1}}{1 + \bar{x}_\alpha + x_c}. \quad (2)$$

Here  $x_c \propto n$  is the collisional coupling coefficient for H–H interactions (Zygelman 2005) and H–e<sup>−</sup> collisions (Smith 1966; Liszt 2001). The middle term describes the Wouthuysen-Field effect, in which absorption and re-emission of Ly $\alpha$  photons mixes the hyperfine states. The coupling coefficient is (Chen & Miralda-Escudé 2004; Hirata 2005)

$$\bar{x}_\alpha = 1.81 \times 10^{11} (1+z)^{-1} \tilde{S}_\alpha J_\alpha, \quad (3)$$

where  $\tilde{S}_\alpha$  is a factor of order unity describing the detailed atomic physics of the scattering process and  $J_\alpha$  is the background flux at the Ly $\alpha$  frequency in units  $\text{cm}^{-2} \text{ s}^{-1} \text{ Hz}^{-1} \text{ sr}^{-1}$ ; the Wouthuysen-Field effect becomes efficient when there is about one photon per baryon near this frequency. It couples  $T_S$  to an effective color temperature  $\tilde{T}_c$  (in most circumstances,  $\tilde{T}_c \approx T_K$ ; Field 1959). We use the numerical fits of Hirata (2005) for  $\tilde{S}_\alpha$  and  $\tilde{T}_c$ .

## 3 THE THERMAL HISTORY

To compute the evolution of  $\delta T_b$ , we therefore need  $T_K(z)$ ,  $J_\alpha(z)$ , and  $\bar{x}_i(z)$ . In the next three sections, we will examine each in turn, beginning with the kinetic temperature. The evolution equation is

$$\frac{dT_K}{dt} = -2H(z)T_K + \frac{2}{3} \sum_i \frac{\epsilon_i}{k_B n}, \quad (4)$$

where the first term on the right hand side is the  $p dV$  work from the expanding universe and  $\epsilon_i$  is the energy input into the gas per second per unit (physical) volume through process  $i$ . We include a number of possible input mechanisms.

### 3.1 Compton Heating

At high redshifts, Compton scattering between CMB photons and the residual free electrons in the IGM dominates. The heating rate is (e.g., Seager et al. 2000)

$$\frac{2}{3} \frac{\epsilon_{\text{comp}}}{k_B n} = \frac{\bar{x}_i}{1 + f_{\text{He}} + \bar{x}_i} \frac{8\sigma_T u_\gamma}{3m_e c} (T_\gamma - T_K), \quad (5)$$

where  $f_{\text{He}}$  is the helium fraction (by number),  $u_\gamma \propto T_\gamma^4$  is the energy density of the CMB, and  $\sigma_T$  is the Thomson cross-section. The first factor occurs because CMB photons scatter off free electrons, but the heat must be shared with all the particles. The efficiency of Compton heating decreases with cosmic time as electrons recombine and  $u_\gamma$  falls; the IGM thermally decouples from the CMB at (Peebles 1993)

$$1 + z_{\text{dec}} \approx 150 (\Omega_b h^2 / 0.023)^{2/5}. \quad (6)$$

Below this point,  $T_K \propto (1+z)^2$ , as appropriate for a thermally isolated expanding gas.

### 3.2 X-ray Heating

The thermal evolution becomes much more complex (and uncertain) once the first luminous sources appear. X-rays from galaxies and quasars likely provide most of the heat for the low-density IGM. Given our large uncertainties about the nature of high-redshift objects, we will take a simple parameterized approach calibrated to nearby starburst galaxies. These objects show a clear

correlation between star formation rate (as measured by the total infrared luminosity) and hard X-ray (2–10 keV) luminosity (Grimm et al. 2003; Ranalli et al. 2003; Gilfanov et al. 2004):

$$L_X = 3.4 \times 10^{40} f_X \left( \frac{\text{SFR}}{1 \text{ M}_\odot \text{ yr}^{-1}} \right) \text{ erg s}^{-1}, \quad (7)$$

where  $f_X$  is a correction factor accounting for the (unknown) differences at high redshifts. Note that we have transformed to the total ( $> 0.2$  keV) X-ray luminosity assuming a spectral index  $\alpha = 1.5$  (where  $L_\nu \propto \nu^{-\alpha}$ ) in this range (Rephaeli et al. 1995). This is only an average index, of course, but errors can be subsumed into the unknown normalization  $f_X$ .

There is of course no rigorous justification for extrapolating this relationship to high redshifts, but it is certainly reasonable. Massive X-ray binaries produce the bulk of high-energy emission in nearby starbursts. Such systems form when the first massive stars die, only a few million years after star formation commences. So they should also be present in high-redshift galaxies (Glover & Brand 2003). Of course, their abundance must change with the metallicity and initial mass function (IMF): if, for example, the IMF is top-heavy,  $f_X$  could be significantly larger than unity. But for the moment we can only speculate about the magnitude of such evolutionary effects.

A second source is inverse-Compton scattering from relativistic electrons accelerated in the supernova remnants. In the nearby universe, only powerful starbursts have strong enough radiation fields for this to be competitive with synchrotron cooling; however, the CMB has  $u_\gamma \propto (1+z)^4$ , so inverse-Compton emission may dominate over synchrotron emission in *all* star-forming environments at high redshift (Oh 2001). We can make a simple estimate of the extra luminosity contributed by these fast electrons. Suppose that a fraction  $\epsilon_e$  of the total supernova energy  $E_{\text{SN}}$  is used to accelerate electrons, and that a fraction  $f_e \sim 0.5$  of this energy is emitted in X-ray photons (this fraction is determined by cooling within the shock; Furlanetto & Loeb 2004). We also let  $\nu_{\text{SN}}$  be the number of supernovae per unit mass of star formation. Then

$$L_X^{\text{SN}} = 1.6 \times 10^{40} f_e \left( \frac{\epsilon_e}{0.05} \frac{\nu_{\text{SN}}}{0.01 \text{ M}_\odot^{-1}} \frac{E_{\text{SN}}}{10^{51} \text{ erg}} \right) \times \left( \frac{\text{SFR}}{1 \text{ M}_\odot \text{ yr}^{-1}} \right) \text{ erg s}^{-1}, \quad (8)$$

where we have substituted  $\epsilon_e \sim 0.05$  as appears to be appropriate for nearby supernova remnants (e.g., Koyama et al. 1995). Thus, if a large fraction of the electron energy is emitted in X-ray photons, inverse-Compton emission from fast electrons can contribute a non-negligible – though not necessarily dominant – fraction of the total emission. Conveniently,  $f_X \sim 1$  still seems reasonable.

Extremely massive ( $> 300 \text{ M}_\odot$ ) Pop III stars<sup>1</sup> could have a wildly different normalization, of course: each pair-instability supernova releases  $\sim 10^{52}$ – $10^{53}$  erg, much more than normal supernovae (Heger & Woosley 2002). The fraction of X-ray binaries may also be significantly larger, or the remnants may form “miniquasars.” Moreover, these stars also produce soft X-rays directly, because they have surface temperatures  $T_{\text{eff}} \sim 10^5$  K (Bromm et al. 2001; Schaerer 2002). To a first approximation, the

<sup>1</sup> Note that we will use “Pop III” to refer exclusively to this very massive case. If Pop III stars have more or less normal initial mass functions, they produce histories close to our Pop II case. We use the massive stars only for contrast with the “standard” histories and do not mean to pass judgment on the relative merits of the different initial mass functions.

stellar spectra are simple blackbodies, in which case  $\sim 0.3\%$  of the total stellar luminosity is emitted in photons with  $E > 0.1$  keV. This would imply  $f_X \gg 1$ . However, photons near  $\sim 0.1$  keV are absorbed relatively quickly, and they affect only the region within  $\lesssim 0.5$  Mpc of galaxies (Sethi 2005; Cen 2006). Thus it is the harder photons with which we are primarily concerned, and these come from nonthermal sources: at  $T_{\text{eff}} = 10^5$  K, only  $\sim 2 \times 10^{-7}$  of the Pop III stellar luminosity lies in photons with  $E > 0.2$  keV.

Because X-ray heating is thus intrinsically non-uniform, we must develop some approximation for our global treatment – in the simplest terms, we must specify the photon energy range that we assume can penetrate into the diffuse IGM. Equation (7) included all photons with  $E > 0.2$  keV. In actuality, all photons with  $E < E_{\text{thick}} = 1.5 \bar{x}_{\text{HI}}^{1/3} [(1+z)/10]^{1/2}$  keV are absorbed within a Hubble length (Oh 2001), so photons near the bottom edge of our range will be absorbed over a relatively small – but by no means negligible – volume. By including soft photons, we are attempting to balance the highly-penetrating hard X-rays with the more localized soft X-rays that likely carry more total energy. Of course, this fluctuating component (e.g., Madau et al. 2004) will lead to non-uniform heating (Sethi 2005). We defer discussion of these fluctuations to future work; our concern here is with understanding the zeroth-order global evolution. Fortunately, uncertainty in the overall effect of inhomogeneity can be subsumed into our much larger uncertainty in  $f_X$  so long as the spectrum is a reasonably shallow power law (as appropriate for nonthermal sources). For example, Glover & Brand (2003) used a method much like our own but took  $f_X \sim 0.2$  because they calibrated to the luminosity in the 2–10 keV band, which implicitly assumes that soft photons are absorbed inside or near their source galaxies.

X-rays deposit energy in the IGM by photoionizing hydrogen and helium; the hot “primary” electron then distributes its energy through three channels: (1) collisional ionization, producing more secondary electrons, (2) collisional excitation of He, which produces a photon capable of ionizing H, and (3) Coulomb collisions with thermal electrons. The relative cross-sections of these processes determine the fraction of X-ray energy going to heating ( $f_{X,h}$ ) and ionization ( $f_{X,\text{ion}}$ ); clearly they depend on both  $\bar{x}_i$  and the initial photon energy. For our calculations, we will use the high energy limit ( $E \gg 0.1$  keV) of Shull & van Steenberg (1985), who fit their results to

$$\begin{aligned} f_{X,h} &= C_1 [1 - (1 - x_i^{a_1})^{b_1}] \\ f_{X,\text{ion}} &= C_2 (1 - x_i^{a_2})^{b_2}. \end{aligned} \quad (9)$$

Here  $C_1 = 0.9971$ ,  $a_1 = 0.2663$ ,  $b_1 = 1.3163$ ,  $C_2 = 0.3908$ ,  $a_2 = 0.4092$ , and  $b_2 = 1.7592$ ; the fits are accurate to  $\lesssim 2\%$  in the range of interest. Although not as good for softer photons, the qualitative behavior is similar: when  $\bar{x}_i$  is small, most of the energy is deposited in ionizations ( $f_{X,h} \approx 0.2$  for  $E = 3$  keV and  $\bar{x}_i = 10^{-3}$ ), but  $f_{X,h} \rightarrow 1$  as  $\bar{x}_i \rightarrow 1$ , because collisions with free electrons become more important.<sup>2</sup>

We are now in a position to estimate the heating rate from X-rays in the early universe. We first assume that the star formation rate is proportional to the rate at which matter collapses into galaxies, which we assume correspond to dark matter halos

<sup>2</sup> Note that here  $x_i$  refers to the ionized fraction in the predominantly neutral gas (outside of HII regions) whose temperature we care about. In the models below, we track this separately from the usual ionized fraction, which instead describes the filling factor of HII regions, by assuming that only X-rays ionize this mostly neutral gas.

with  $m > m_{\min}$ , where  $m_{\min}$  is a (redshift-dependent) minimum mass. We will typically take  $m_{\min} = m_4$ , where  $m_4$  has a virial temperature  $T_{\text{vir}} = 10^4$  K (the threshold for atomic cooling; Barkana & Loeb 2001). We define  $f_{\text{coll}}$  to be the fraction of matter in collapsed halos with  $m > m_{\min}$ ; for the Press & Schechter (1974) mass function, it takes the simple analytic form

$$f_{\text{coll}} = \text{erfc} \left[ \frac{\delta_c(z)}{\sqrt{2}\sigma(m_{\min})} \right], \quad (10)$$

where  $\delta_c$  is the linear overdensity at virialization and  $\sigma^2(m)$  is the variance of the density field when smoothed on scale  $m$ . By equation (7), the X-ray emissivity is proportional to the star formation rate and hence to  $df_{\text{coll}}/dt$ ; the result is

$$\frac{2}{3} \frac{\epsilon_X}{k_B n H(z)} = 10^3 \text{ K } f_X \left( \frac{f_\star}{0.1} \frac{f_{X,h}}{0.2} \frac{df_{\text{coll}}/dz}{0.01} \frac{1+z}{10} \right), \quad (11)$$

where  $f_\star$  is the star formation efficiency. We immediately see that X-ray heating should be quite rapid, provided that  $f_X \gtrsim 0.1$ .

Of course, our assumption that  $\epsilon_X \propto df_{\text{coll}}/dt$  may be wrong because (for example) some exotic process produces X-rays, or because quasars are common, or simply because  $f_\star$  is not a constant. However, unless the process of interest is uncorrelated with galaxy formation, it will not differ dramatically from that we have discussed. On the other hand, quasars could strongly increase the normalization of  $f_X$ . We have chosen to ignore this possibility because extrapolating the known population of bright quasars to higher redshifts yields an X-ray background with negligible effects on the IGM (Venkatesan et al. 2001). A number of models posit an entirely new population of “miniquasars” (e.g., Madau et al. 2004; Ricotti et al. 2005), but we will conservatively ignore them. We briefly discuss how such miniquasars could affect our conclusions in §8.

### 3.3 Ly $\alpha$ Heating

As photons redshift into the Lyman-series resonances, they scatter off of neutral hydrogen atoms in the IGM and deposit energy in the gas through atomic recoil. While initially thought to be an important heat source (Madau et al. 1997), Chen & Miralda-Escudé (2004) and Rybicki (2006) showed that the energy deposition rate in repeated Ly $\alpha$  scatterings is actually extremely small because the photons quickly establish equilibrium with the gas (see also Furlanetto et al. 2006 for a discussion of the approach to equilibrium). The heating rate from higher Lyman resonances is also small because those photons are quickly transformed into either Ly $\alpha$  photons or continuum photons that easily escape to infinity (Pritchard & Furlanetto 2005). We therefore neglect this mechanism.

### 3.4 Shock Heating

Finally, we must consider heating from shocks in the IGM. At low redshifts, shocks play an integral role in its temperature structure (Cen & Ostriker 1999; Davé et al. 2001). The shock networks surrounding filaments and halos can be quite complex (Miniati et al. 2000; Kang et al. 2005), but their characteristic properties are easy to estimate. The typical shock that has just collapsed at redshift  $z$  will have a peculiar velocity equal to the total distance it has collapsed divided by the age of the Universe,  $v_{\text{sh}} \approx H(z)R_{\text{nl}}(z)$ , where  $R_{\text{nl}}$  is the (physical) nonlinear length scale (Cen & Ostriker

1999). For a strong shock in a monatomic gas, the corresponding postshock temperature is

$$T_{\text{sh}} = \frac{3\mu m_p}{16k_B} v_{\text{sh}}^2 \approx \frac{3\mu m_p}{16k_B} H^2(z) R_{\text{nl}}^2(z), \quad (12)$$

where  $\mu$  is the mean molecular weight in atomic units. This yields  $T_{\text{sh}} \sim 10^7$  K at the present day (Cen & Ostriker 1999), comparable to the results of numerical simulations. On the other hand  $T_{\text{sh}} \sim 10^4$  K at  $z \sim 3$ , close to the mean temperature of a photoionized medium (Furlanetto & Loeb 2004). Thus large-scale structure shocks decrease in importance at moderate redshifts.

However, *before* reionization they are also important, because without photoheating  $T_K$  can be small and the IGM sound speed may be much less than  $v_{\text{sh}}$ . Unfortunately, studying this regime requires extremely high resolution numerical simulations, and the current generation appears to disagree on their significance. Gnedin & Shaver (2004) found IGM shocks to be the most important factor in determining  $\delta T_b$  at  $z \lesssim 15$ , but other simulations suggest that filament shocks have a relatively modest effect (comparable to the signal from minihalos; Kuhlen et al. 2006; Shapiro et al. 2005). One possible reason for the discrepancy is that the latter two studies assumed that only overdense gas could be observed against the CMB and so only included shocks bounding the cosmic web. Gnedin & Shaver (2004), on the other hand, assumed that the entire IGM was visible because of Ly $\alpha$  coupling. Thus it is possible that the tiny sound speed in the IGM allows a population of weak shocks to exist *outside* the cosmic web. Unfortunately, weak shocks in the low density IGM may be difficult to resolve properly in simulations. Another alternative is that the differences occurred because the studies focused on different redshift regimes.

For now, we will assume the latter and use the simple model of Furlanetto & Loeb (2004) to estimate the effect of shocks in the cosmic web (see also Nath & Silk 2001; Valageas et al. 2002). This prescription assumes that shocks form around a region once its mean linearized density exceeds  $\delta_{\text{sh}} = 1.06$ . This is equivalent to assuming that they appear when spherical perturbations “turnaround” and break off from the Hubble flow (i.e., when the flow begins to converge). This spherical picture is approximate, but it provides a simple criterion to estimate the fraction of mass that has been shocked on its way to halo formation. Conveniently, at turnaround, the physical velocity is of course zero, so the peculiar velocity is almost precisely  $v_{\text{sh}} \approx H(z)R_{\text{nl}}(z)$ . Thus it reproduces the characteristic temperature of  $z = 0$  shocks. In the same way as the Press & Schechter (1974) mass function, it also yields the distribution of shock temperatures at any epoch.

Thus, by analogy to equation (10), the fraction of gas that has been shocked to a temperature  $T > T_{\text{sh}}$  is

$$f_{\text{sh}}(> T_{\text{sh}}) = \text{erfc} \left[ \frac{\delta_{\text{sh}}(z)}{\sqrt{2}\sigma(T_{\text{sh}})} \right], \quad (13)$$

where  $T_{\text{sh}}$  is related to the mass of the underlying perturbation via equation (12). For example, the mass corresponding to a shock with  $T_{\text{sh}} = T_\gamma$  is  $M_\gamma \approx 4.3 \times 10^5 M_\odot$ , which is somewhat greater than the minimum collapse mass (the so-called “filter mass;” Gnedin & Hui 1998) – though note that  $\delta_{\text{sh}} < \delta_c$  so more gas will be in the shocked phase than in collapsed objects of a comparable mass. For our model, we will simply compute the fraction  $f_{\text{sh}}$  of gas that has been heated to  $T_K > T_\gamma$ . We will assume that this gas emits strongly relative to the CMB ( $T_S \gg T_\gamma$ ), while the rest remains at the mean temperature (without shocks). Note that, once X-rays have heated the IGM above  $T_\gamma$ , shock heating will become less significant than our prescription assumes; however, in

that regime the shocked gas and background IGM emit at nearly the same level and so shocks have almost no observable effect.

We emphasize that this treatment is meant to include only shocks that are part of structure formation (sheets, filaments, and halos). As described above, there may be a population of weaker shocks in the low-density IGM that deposit a significant amount of thermal energy there. In the language of our model, these would correspond to shocks that appear *before* turnaround due to random IGM flows. Our model may thus underestimate  $T_K$  at early times and overestimate the amplitude and duration of absorption. But, as we will see, X-ray heating generally becomes significant at  $z \gtrsim 15$ , when such perturbations would presumably be significantly smaller than those of Gnedin & Shaver (2004).

#### 4 THE SPIN TEMPERATURE

Once  $T_K$  is known, the next step is to compute the spin temperature of the gas. We include H-H collisions (Zygelman 2005), H-e<sup>-</sup> collisions (Smith 1966; Liszt 2001), and the Wouthuysen-Field effect (Wouthuysen 1952; Field 1958; Hirata 2005) as described in §2. Collisions are unimportant for the low-density IGM during the epochs of interest,<sup>3</sup> so the Wouthuysen-Field mechanism is therefore the most important factor. Its strength depends on the soft-UV radiation background, for which we will construct a simple, easily parameterized model. We again assume that young stars dominate the flux, so that we can write the comoving emissivity at frequency  $\nu$  is

$$\epsilon(\nu, z) = f_\star \bar{n}_b^0 \epsilon_b(\nu) \frac{df_{\text{coll}}}{dt}. \quad (14)$$

The function  $\epsilon_b(\nu)$  is the number of photons produced in the frequency interval  $\nu \pm d\nu/2$  per baryon incorporated into stars. For spin temperature coupling, we are interested only in photons between Ly $\alpha$  and the Lyman-limit.<sup>4</sup> We use the spectral models of Barkana & Loeb (2005b), which fit a power law between each Lyman-series resonance. For Population III stars, a total of  $N_\alpha = 4800$  photons are produced per baryon in the interval  $(\nu_\alpha, \nu_{\text{LL}})$ , with a relatively flat spectral distribution (Bromm et al. 2001). For continuously forming low-metallicity Population II stars,  $N_\alpha = 9690$  photons are produced per baryon, with the spectrum falling steeply past the Ly $\beta$  resonance (Leitherer et al. 1999).

The average Ly $\alpha$  background is then

$$\begin{aligned} J_\alpha(z) &= \sum_{n=2}^{n_{\text{max}}} J_\alpha^{(n)}(z) \\ &= \sum_{n=2}^{n_{\text{max}}} f_{\text{rec}}(n) \int_z^{z'_n} dz' \frac{(1+z')^2}{4\pi} \frac{c}{H(z')} \epsilon(\nu'_n, z'), \end{aligned} \quad (15)$$

<sup>3</sup> Unless, that is, X-ray heating is extremely strong and renders  $\bar{x}_i \gtrsim 0.03$  (Nusser 2005).

<sup>4</sup> Here we ignore Lyman-line photons produced inside galaxies as well as line photons produced following IGM ionizations. The former is a reasonable assumption because these photons rapidly redshift out of resonance and hence only affect a small fraction of the IGM (much of which is predominantly ionized). The second is an excellent approximation for Pop II stars but less good for Pop III stars, because of their hard spectra. Nevertheless, such photons also rapidly redshift out of resonance near the edge of the HII regions.

where  $J_\alpha^{(n)}$  is the background from photons that originally redshift into the Ly $n$  resonance,  $\nu'_n$  is the frequency at redshift  $z'$  that redshifts into that resonance at redshift  $z$ ,

$$\nu'_n = \nu_n \frac{(1+z')}{(1+z)}, \quad (16)$$

and

$$\frac{1+z'_n}{1+z} = \frac{1-(n+1)^{-2}}{1-n^{-2}} \quad (17)$$

is the largest redshift from which a photon can redshift into it. The factor  $f_{\text{rec}}(n)$  is the fraction of the resulting Ly $n$  photons that actually cascade through Ly $\alpha$  and induce strong coupling (Hirata 2005; Pritchard & Furlanetto 2005). We truncate the sum at  $n_{\text{max}} = 23$  (following Barkana & Loeb 2005b), although the closely-spaced  $n \gg 1$  levels contribute only a small fraction of the total flux. Finally, we compute the coupling coefficient  $\bar{x}_\alpha$  from equation (3).

For estimation purposes, we can approximate equation (15) as

$$J_\alpha \approx \frac{c}{4\pi} \bar{f}_{\text{rec}} f_\star \bar{n}_b^0 \Delta f_{\text{coll}} \frac{N_\alpha}{\Delta\nu} (1+z)^2. \quad (18)$$

Here  $\bar{f}_{\text{rec}}$  is the average probability that a photon in the interval  $(\nu_\alpha, \nu_{\text{LL}})$  is converted into a Ly $\alpha$  photon. It is  $\bar{f}_{\text{rec}} = 0.63$  and  $0.72$  for our Pop III and Pop II spectra (Pritchard & Furlanetto 2005). We have approximated the spectrum as constant (so that  $\epsilon_b \sim N_\alpha/\Delta\nu$ , where  $\Delta\nu = \nu_{\text{LL}} - \nu_\alpha$ ) and let  $\Delta f_{\text{coll}} \sim f_{\text{coll}}$  be the spectrum-weighted collapse fraction over the appropriate redshift intervals in equation (15).

#### 5 THE IONIZATION HISTORY

The next step in understanding the global history of the 21 cm signal is  $\bar{x}_i(z)$ . This has been a subject of extensive study over the past three decades (see, e.g., Barkana & Loeb 2001; Haiman 2004; Ciardi & Ferrara 2005 for recent reviews). As such, we will not attempt to explore all of its aspects. We will again examine a simple model encapsulating the major features in the global evolution.

We associate reionization with the star formation rate in a similar way to the Ly $\alpha$  and X-ray backgrounds (see eqs. [11] and [14]). We write

$$\frac{d\bar{x}_i}{dt} = \zeta(z) \frac{df_{\text{coll}}}{dt} - \alpha_A C(z, x_i) \bar{x}_i(z) \bar{n}_e(z), \quad (19)$$

where  $\zeta$  is an ionizing efficiency parameter,  $\alpha_A = 4.2 \times 10^{-13} \text{ cm}^3 \text{ s}^{-1}$  is the recombination coefficient at  $T = 10^4 \text{ K}$ ,<sup>5</sup>  $C \equiv \langle n_e^2 \rangle / \langle n_e \rangle^2$  is the clumping factor,  $\bar{n}_e$  is the average electron density in ionized regions, and  $\zeta$  is an ionizing efficiency parameter. The first term on the right hand side is the source term for ionizing photons and the second term is a sink describing recombinations.

We must now specify  $\zeta$ ,  $m_{\text{min}}$  (for  $f_{\text{coll}}$ ), and  $C$ . The ionizing efficiency can be written

$$\zeta = A_{\text{He}} f_\star f_{\text{esc}} N_{\text{ion}}, \quad (20)$$

where  $f_{\text{esc}}$  is the fraction of ionizing photons that escape their host galaxy into the IGM,  $N_{\text{ion}}$  is the number of ionizing photons per baryon produced in stars, and  $A_{\text{He}}$  is a correction factor for helium. With the exception of  $A_{\text{He}}$ , all of these parameters are highly

<sup>5</sup> Note that we use the case-A value, which essentially amounts to assuming that ionizing photons are absorbed inside dense, neutral systems (Miralda-Escudé et al. 2000).

uncertain. The star formation efficiency depends on the dynamics of star formation in young galaxies,  $f_{\text{esc}}$  depends on the distribution of gas, dust, and stars within galaxies, and  $N_{\text{ion}}$  depends on the stellar IMF and metallicity. We will therefore content ourselves with representative values of these parameters in our calculations (see the discussion in Furlanetto et al. 2006 for more information).

Of course, both  $\zeta$  and  $m_{\text{min}}$  could evolve with time because of feedback. For example, metal enrichment could decrease  $\zeta$  if Pop II stars are less efficient than their Pop III progenitors, or  $m_{\text{min}}$  could increase because of photoheating during reionization (Rees 1986; Efstathiou 1992; Thoul & Weinberg 1996; Kitayama & Ikeuchi 2000; but see Dijkstra et al. 2004). Feedback is one promising method to slow reionization and reconcile the SDSS quasar data with *WMAP*, but the mechanisms at play and their interactions are essentially unconstrained. For our purposes, the important question is how they affect the global reionization history. Early efforts suggested that they might introduce sharp features such as “double reionization” (Cen 2003b; Wyithe & Loeb 2003a). However, this requires a sharp drop in the ionizing efficiency that is synchronized across the entire Universe. That is difficult to arrange when the inhomogeneities inherent to local feedback mechanisms are included (Furlanetto & Loeb 2005). Instead, feedback is likely to prolong reionization or introduce a “stalling” phase. We will show some examples generated using the feedback models of Furlanetto & Loeb (2005) to illustrate its effects.

The clumping factor can, in principle, be computed through numerical simulations with radiative transfer. Unfortunately, that requires fully resolving small-scale structure in the IGM as well as its evolution throughout reionization. Moreover,  $C$  depends on how the IGM is ionized – for instance, whether low-density gas is ionized first or whether many photons are consumed ionizing dense blobs when  $\bar{x}_i$  is still small (Furlanetto & Oh 2005). Thus  $C$  must be recalculated for each different set of model parameters. Unfortunately, simulations have not yet achieved these goals. Following our usual policy, we will therefore use a simple analytic model (Miralda-Escudé et al. 2000); in this prescription, voids are ionized first. This probably underestimates the mean recombination rate, so reionization may be a bit slower than our models predict (and begin a bit later). On the other hand, simulations suggest that recombinations do not dramatically slow reionization, even if minihalos are included (Ciardi et al. 2005). Note that when recombinations are slow, equation (19) can be approximated as

$$\bar{x}_i \approx \frac{\zeta f_{\text{coll}}}{1 + \bar{n}_{\text{rec}}}, \quad (21)$$

where  $\bar{n}_{\text{rec}}$  is the mean cumulative number of recombinations per hydrogen atom.

## 6 CRITICAL POINTS IN THE 21 CM HISTORY

Now that we have assembled the relevant physics, we are ready to construct some plausible histories. But first it is useful to identify three “critical points” in the 21 cm history: the redshift  $z_h$  at which the IGM is heated above  $T_\gamma$ , the redshift  $z_c$  at which the Wouthuysen-Field mechanism couples first  $T_S$  and  $T_K$  (when  $\tilde{x}_\alpha = 1$ ), and the redshift of reionization  $z_r$ . Their relative timing determines the structure of the 21 cm spectrum.

The most important question is whether  $z_c$  occurs before the other two transitions: if not, the IGM will remain invisible. We can compute the collapse fraction (or more precisely  $\Delta f_{\text{coll}}$ ) required to achieve  $\tilde{x}_\alpha = 1$  from equation (18). Substituting this into equa-

tion (11), integrated over time, we have the net X-ray heat input  $\Delta T_c$  at  $z_c$ :

$$\frac{\Delta T_c}{T_\gamma} \sim 0.08 f_X \left( \frac{f_{X,h}}{0.2} \frac{f_{\text{coll}}}{\Delta f_{\text{coll}}} \frac{9690}{N_\alpha} \frac{1}{\bar{S}_\alpha} \frac{0.6}{\bar{f}_{\text{rec}}} \frac{0.023}{\Omega_b h^2} \right) \times \left( \frac{20}{1+z} \right)^3. \quad (22)$$

Note that  $\Delta T_c$  is independent of  $f_\star$  because both the coupling and heating rates are proportional to the star formation rate (by assumption, of course). Interestingly, for fiducial (Pop II) parameters  $z_c$  should occur somewhat before  $z_h$  (see also the simple models of Chen & Miralda-Escudé 2004; Hirata 2005). For Pop III stars,  $N_\alpha$  is a factor of two smaller and  $f_X$  may be significantly larger than unity, in which case absorption would be much less important. Thus the presence or absence of a strong and extended absorption epoch offers a useful probe of high-redshift star formation.

A similar estimate of the ionization fraction at  $z_c$  yields

$$\bar{x}_{i,c} \sim 0.05 \left( \frac{f_{\text{esc}}}{1 + \bar{n}_{\text{rec}}} \frac{N_{\text{ion}}}{N_\alpha} \frac{f_{\text{coll}}}{\Delta f_{\text{coll}}} \frac{1}{\bar{S}_\alpha} \frac{0.6}{\bar{f}_{\text{rec}}} \frac{0.023}{\Omega_b h^2} \right) \times \left( \frac{20}{1+z} \right)^2. \quad (23)$$

For Pop II stars,  $N_{\text{ion}}/N_\alpha \approx 0.45$ ; thus even in the worst case ( $f_{\text{esc}} = 1$  and  $\bar{n}_{\text{rec}} = 0$ ) coupling would become efficient during the initial stages of reionization. However, Pop III stars have much harder spectra and  $N_{\text{ion}}/N_\alpha \approx 7$ .<sup>6</sup> In principle, it is therefore possible for Pop III stars to reionize the universe *before*  $z_c$ . This requires a small clumping factor, relatively late reionization ( $z \lesssim 10$ ), and  $f_{\text{esc}} \approx 1$ . There is some theoretical motivation for such a large escape fraction in the earliest generation of galaxies (Whalen et al. 2004), but maintaining that in larger galaxies seems unlikely (as might widespread and dominant Pop III star formation at  $z < 10$ ). More conventional histories, in which  $f_{\text{esc}} \lesssim 0.2$  or  $z_r \gtrsim 12$  for Pop III stars, predict strong coupling throughout reionization (cf. Ciardi & Madau 2003).

Finally, it is interesting to check whether we will see the IGM in absorption or emission during reionization. Combining equations (11) and (21), we find that the total heat input as a function of  $\bar{x}_i$  is

$$\frac{\Delta T(\bar{x}_i)}{T_\gamma} \sim \left( \frac{\bar{x}_i}{0.025} \right) \left( f_X \frac{f_{X,h}}{f_{\text{esc}}} \frac{4800}{N_{\text{ion}}} \frac{10}{1+z} \right) (1 + \bar{n}_{\text{rec}}). \quad (24)$$

Thus, provided  $f_X \gtrsim 1$  and Pop II stars dominate, it is safe to assume that the IGM is much warmer than the CMB throughout reionization. However, because Pop III stars have much higher ionizing efficiencies, it is possible for X-ray heating to become significant only when  $\bar{x}_i \gtrsim 0.2$ ; in this case we would be able to see the early stages in absorption so long as  $f_X$  remains small. This would be exciting in that it would add extra structure to the reionization signal, but it would also make isolating  $\bar{x}_i(z)$  more difficult.

<sup>6</sup> Note that Fig. 1 of Ciardi et al. (2003) seems to suggest much smaller ratios for Pop III stars; this is because they report the number of photons *per frequency interval*. The frequency range between Ly $\alpha$  and the Lyman limit is much smaller than that available to ionizing photons, which accounts for the difference.

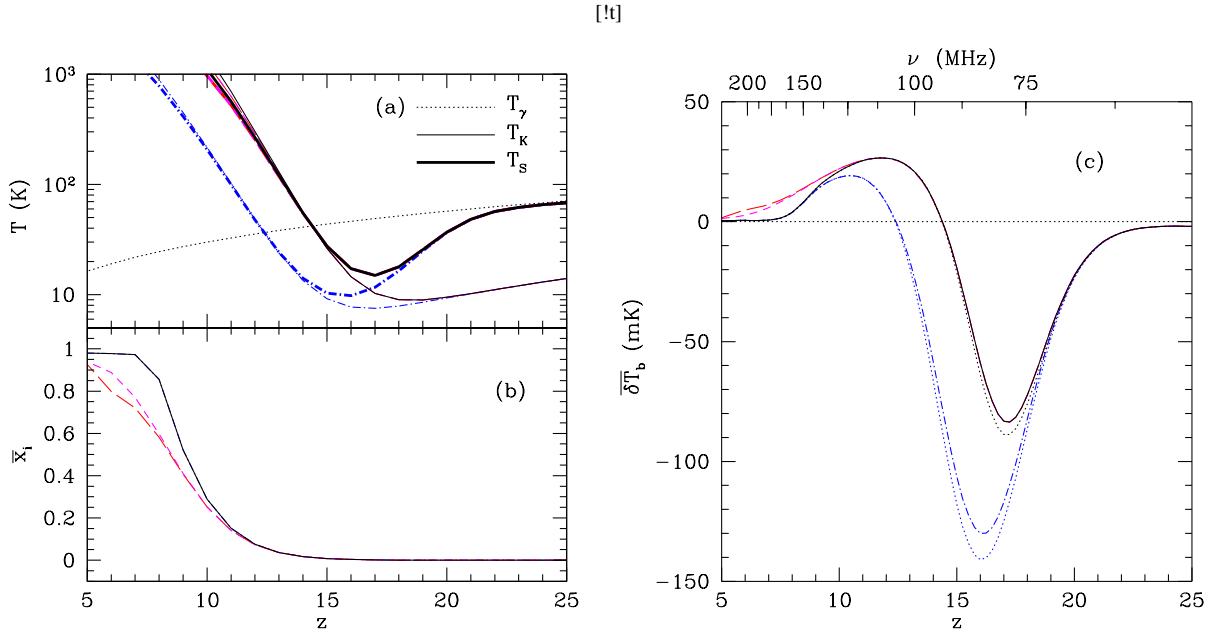


**Figure 1.** Global IGM histories for Pop II stars. The solid curves take our fiducial parameters. The dot-dashed curves take  $f_X = 0.2$ . The short- and long-dashed curves include photoheating feedback (see text). (a): CMB, gas kinetic, and spin temperatures (dotted, thin, and thick curves, respectively). (b): Ionized fraction. (c): Differential 21 cm brightness temperature against the CMB. In this panel, the two dotted lines show  $\delta T_b$  if shock heating is ignored.

## 7 GLOBAL HISTORIES

We will now construct some example histories using the prescriptions given in §3–5. Of course, given the uncertainties in each of the parameters, making firm predictions is all but impossible. But we can highlight the possible range of features. We will necessarily neglect a number of potentially important effects (such as metal enrichment and the evolution of the  $H_2$  cooling efficiency), but we hope that our histories are nevertheless representative of the possibilities.

### 7.1 Pop II Stars

We begin with a fiducial set of Pop II parameters. We take  $m_{\min} = m_4$ ,  $f_* = 0.1$ ,  $f_{\text{esc}} = 0.1$ ,  $f_X = 1$ ,  $N_{\text{ion}} = 4000$ , and  $N_\alpha = 9690$ . (Thus  $\zeta = 40$  for this model.) The solid curves in Figure 1 show the resulting global history. In panel (a), the dotted curve is  $T_\gamma$ , the thin curves are  $T_K$ , and the thick curves are  $T_S$  (note that they always interpolate between  $T_\gamma$  and  $T_K$ ).

Figure 1b shows the ionization history. Without feedback, it increases smoothly and rapidly over a redshift interval of  $\Delta z \sim 5$ . For these parameters, reionization is essentially complete at  $z_r \sim 7$ . Other values of  $\zeta$  move  $z_r$  back and forth but do not strongly affect its width in redshift space. Changing  $f_*$  affects all three processes (nearly) equally: it simply moves the entire curve forward or backward in redshift. Note that the evolution slows somewhat at  $\bar{x}_i \gtrsim 0.8$  and never quite reaches complete reionization; this is because the clumping factor  $C$  increases rapidly as  $\bar{x}_i \rightarrow 1$  (Miralda-Escudé et al. 2000). The dashed curves in this panel use photoheating feedback to slow reionization. Each assumes that the minimum virial temperature increases to  $T_h = 2 \times 10^5$  K in ionized regions, near the upper limit of theoretical expectations (Dijkstra et al. 2004). All other parameters are assumed to remain constant in photoheated regions. The two curves

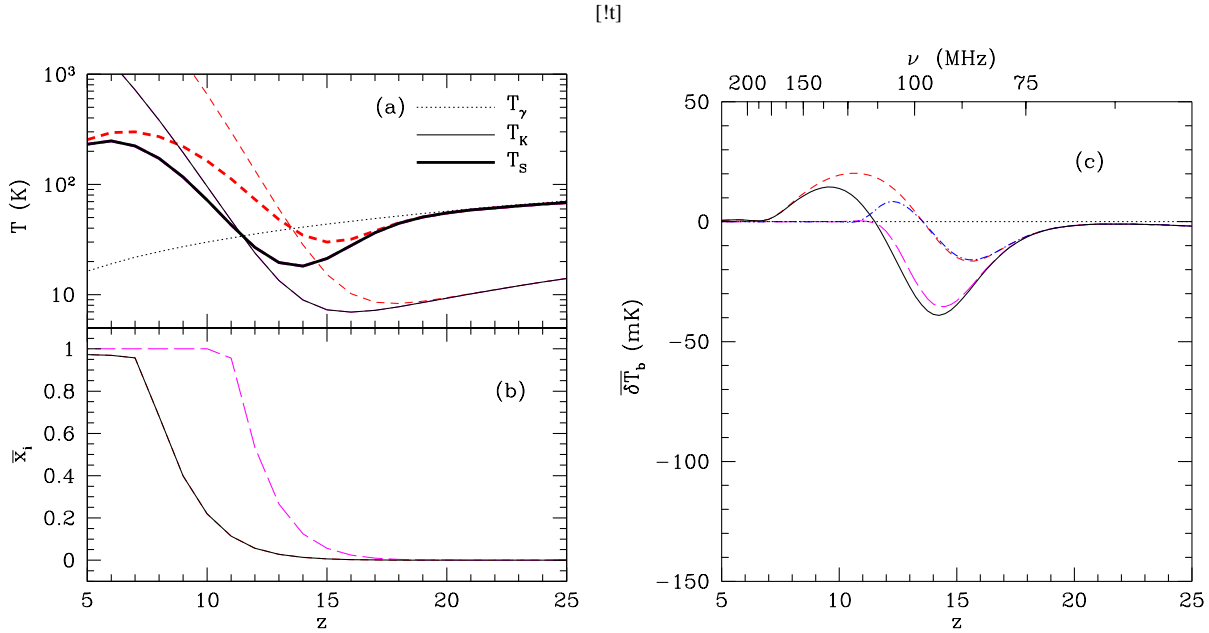
choose different prescriptions for the effective volume in which the feedback occurs; they bracket the possible effects of photoheating (Furlanetto & Loeb 2005).<sup>7</sup> Clearly,  $\bar{x}_i$  evolves monotonically even with this relatively powerful negative feedback. It does, however, slow the pace of reionization when  $\bar{x}_i \gtrsim 0.5$ , spreading it over a significantly longer time interval.<sup>8</sup>

Figure 1c shows the 21 cm brightness temperature increment  $\delta T_b$  relative to the CMB. Here for convenience we have also labeled the corresponding observed frequency  $\nu = \nu_{21}/(1+z)$ , where  $\nu_{21} = 1420$  MHz. The signal clearly has interesting structure. The most robust feature is the  $\sim 30$  mK drop in  $\delta T_b$  during reionization. For our fiducial parameters (and without feedback), that spans a frequency interval of  $\sim 35$  MHz. In this model, recombinations are slow (delaying reionization by only  $\Delta z \approx 1$ ) and  $\bar{x}_i$  is essentially proportional to  $f_{\text{coll}}$ . Thus, unless the ionizing efficiency *increases* throughout reionization because of some positive feedback mechanism (or if more massive galaxies drive reionization; Furlanetto et al. 2006), the signal is unlikely to have a much larger gradient during reionization. But with feedback, it can be significantly smaller: in that case,  $\delta T_b$  falls to zero over  $\Delta z \approx 8$  ( $\sim 60$  MHz here). It is this gradient that might allow us to isolate the cosmological signal, so feedback will make its detection rather more difficult.

A stronger feature appears near  $z_c$  and  $z_h$ . At  $z \gtrsim 20$ , the IGM is nearly invisible even though  $T_K \ll T_\gamma$ . Once the first galaxies form, the Wouthuysen-Field effect becomes important and  $T_S$

<sup>7</sup> In detail, the short-dashed curve assumes that the photoheated volume is identical to the ionized volume, while the long-dashed curve calculates the photoheated volume without including recombinations. See Furlanetto & Loeb (2005).

<sup>8</sup> In fact, with these parameters feedback pushes  $z_r \lesssim 5$ , which is ruled out observationally. But that is of no consequence to us because we only wish to examine its qualitative effects on the 21 cm signal.



**Figure 2.** Global IGM histories for very massive Pop III stars. Panels are the same as in Fig. 1. The solid curve takes our fiducial Pop III parameters (without feedback). The long-dashed lines take  $f_{\text{esc}} = 1$ , the short-dashed lines take  $f_X = 5$ , and the dot-dashed line (shown only in *c*) assumes  $f_{\text{esc}} = 1$  and  $f_X = 5$ .

drops rapidly. Because  $N_\alpha$  is large for Pop II stars, efficient coupling precedes the heating transition, allowing a relatively strong absorption signal ( $\delta T_b \approx -80$  mK) to appear by  $z \sim 20$ . Absorption persists until  $z \sim 15$  (or  $\nu \sim 90$  MHz) before fading into emission. Thus, for these fiducial parameters, the universe is cold when coupling becomes strong, but it still heats up well before reionization begins in earnest. The absorption epoch can therefore teach us about the appearance and spectral properties of the first sources of light in the universe (Tozzi et al. 2000; Sethi 2005), especially the relative importance of Wouthuysen-Field coupling and X-ray heating. This era also produces much sharper features than reionization itself: the signal changes by  $\sim 110$  mK over  $\Delta z \approx 5$  (or  $\Delta \nu \approx 20$  MHz at such high redshifts). Thus, even though the foregrounds are also much larger at the lower frequencies, the early evolution may not be much harder to identify (especially if feedback substantially slows reionization).

Note that our model predicts a significantly stronger absorption epoch than Chen & Miralda-Escudé (2004); the difference lies in the assumed  $f_X$  and in their assumption of a *linearly* increasing emissivity throughout reionization. In reality, structure formation proceeds exponentially at high redshifts, so the X-ray (and ionizing) luminosities most likely decline much more rapidly with redshift than assumed in their model. This permits a longer epoch of absorption.

The other curves in Figure 1 illustrate how the evolution changes with some of our input assumptions. First, the dot-dashed curve assumes  $f_X = 0.2$  (near the value of Glover & Brand 2003). This has no effect on  $\bar{x}_i$ , but it delays the heating transition by  $\Delta z \sim 3$ . As a result,  $T_S$  remains relatively close to  $T_\gamma$  during the beginning of reionization, and  $\delta T_b$  never reaches its peak value in emission. On the other hand, the absorption trough is deeper, though it is still confined to  $z \gtrsim 15$ . Also, we emphasize that the IGM remains visible throughout reionization, even when  $T_S \lesssim T_\gamma$ .

The two dotted curves in panel (c) show  $\delta T_b$  if we ignore

shock heating. In this case, all of the IGM material remains cold. At the high redshifts ( $z \gtrsim 15$ ) that are relevant here, shock heating in filaments affects  $\lesssim 10\%$  of the IGM, so its effects on  $\delta T_b$  are modest. If weak shocks do occur outside of collapsing structures, the absorption epoch will be much weaker. Moreover, if heating is delayed until lower redshifts where structure formation has progressed much further, shocks should have a much larger effect (Gnedin & Shaver 2004; Furlanetto & Loeb 2004).

## 7.2 Population III Stars

Figure 2 shows similar histories for Pop III stars. Here we take fiducial parameters (shown by the solid curves)  $m_{\text{min}} = m_A$ ,  $f_* = 0.01$ ,  $f_{\text{esc}} = 0.1$ ,  $f_X = 1$ , and  $N_{\text{ion}} = 30,000$ , yielding  $\zeta = 30$ ; reionization ends at  $z \approx 7$  in this case, ignoring feedback. The thermal history is similar to the Pop II case, except that the coupling and heating transitions are much more closely spaced in time because Pop III stars have relatively few soft-UV photons per high energy photon. As a result,  $T_S \rightarrow T_K$  occurs just about when  $T_K \sim T_\gamma$ . Thus, if Pop III stars dominate, the absorption epoch will likely be considerably weaker – with a peak signal  $|\delta T_b| \lesssim 50$  mK. In general, with Pop III stars, we find that the time interval over which each quantity evolves is similar to the Pop II case, but the peak signals are up to a factor of two weaker because their spectra push the three transition points closer together. Thus detecting the global signal will be somewhat harder if massive Pop III stars dominate throughout reionization.

The other curves use different input parameters. The long-dashed curves take  $f_{\text{esc}} = 1$  (which may be appropriate for the first stars, Whalen et al. 2004, although it is likely an overestimate in larger galaxies). In this case the universe is obviously ionized much earlier, but the thermal history remains the same. As a result, reionization occurs while the IGM is still cold (see §6). This would complicate the interpretation of  $\delta T_b(z)$  (because tempera-

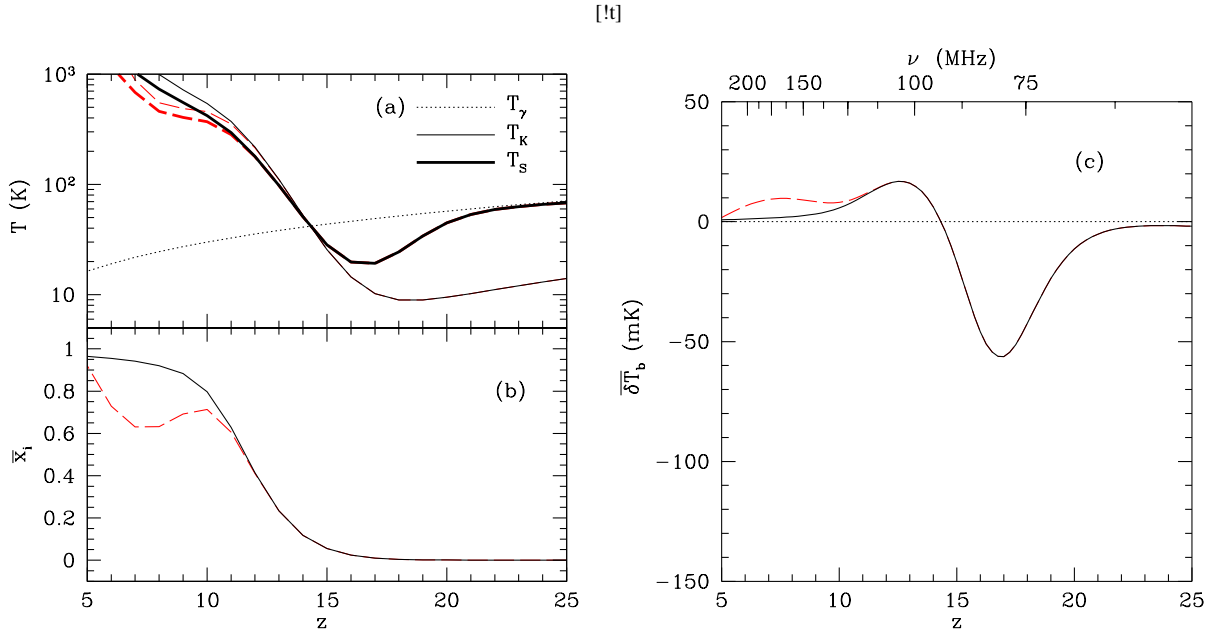


**Figure 3.** Global IGM histories for a two-population model. Panels are the same as in Fig. 1. Both sets of curves assume Pop III stars form in cold regions and Pop II stars form in hot regions (each with our fiducial parameters, except that  $f_\star = 0.1$  for Pop III stars).

ture fluctuations could be significant) but actually makes the reionization signal slightly stronger. The more important point is that the Wouthuysen-Field effect is already strong, so fluctuations will appear throughout reionization: even though  $N_{\text{ion}}/N_\alpha \approx 7$  for these stars, coupling precedes reionization because each Ly $\alpha$  photon is scattered many times. As suggested by equation (23), arranging it so that  $z_c < z_r$  requires extremely unusual parameters, so it is almost impossible to imagine that the IGM would be invisible during reionization.

The short-dashed curves assume  $f_X = 5$ . This strongly increases the heating rate, further decreasing the strength and duration of the absorption epoch. On the other hand, this choice cleanly separates the reionization and absorption epochs and yields a brief period where  $\bar{\chi}_i$  is small but the IGM strongly emits. It gives a similar total heating rate to Hirata (2005), who also predict weak absorption.

Finally, the dot-dashed curve (shown only in panel c) takes  $f_{\text{esc}} = 1$  and  $f_X = 5$ . This is, in many ways, a “worst case scenario” for studying reionization, because it compresses all of our critical points into a short time interval. Nevertheless, there remains interesting structure during and even before reionization. The difference is that separating the effects of  $T_S$ ,  $T_K$ , and  $\bar{\chi}_i$  will be more difficult.

### 7.3 A Dual Population History

In Figure 3, we exaggerate the strength of the photoheating feedback transition by assuming that Pop III stars form in “cold” regions while Pop II stars form in hot regions. Both populations take our fiducial parameters except that we set  $f_\star = 0.1$  for Pop III stars. Thus the ionizing efficiency declines from  $\zeta^{\text{III}} = 300$  to  $\zeta^{\text{II}} = 40$  during photoheating, and  $m_{\text{min}}$  simultaneously increases. There is no real physical justification for conflating the metallicity transition with photoheating – in fact it is much more gradual than photoheating and requires fine-tuning to synchronize enrichment and

reionization (Furlanetto & Loeb 2005) – but it provides a simple way to implement exceptionally strong feedback. As in Figure 1, the solid and dashed curves bracket the effectiveness of photoheating feedback. In the fast case, there is a short period in which  $\bar{\chi}_i$  overshoots because of the dramatic decline in ionizing efficiency between the Pop III and Pop II stars. The resulting recombination epoch is nevertheless shallow, and producing true “double reionization” scenarios requires pushing parameters in even more uncomfortable directions.

Nevertheless, Figure 3 shows that strong feedback can dramatically slow the later stages of reionization. For obvious reasons, photoheating feedback becomes important when  $\bar{\chi}_i \sim 0.5$ . Thus the gradient remains more or less unchanged during the first half of reionization (and the absorption epoch is completely unaffected), but it decreases strongly in the middle stages. Any potential “recombination epoch” is also difficult to see, because  $\bar{\chi}_i$  changes by only  $\sim 15\%$  over  $\Delta z \sim 4$  (yielding  $d\delta T_b/d\nu \sim 0.1$  mK MHz $^{-1}$ ). On the other hand, if feedback is fast, the late stages of reionization are completed entirely by the Pop II objects and so have as large a gradient as the single-population models. Thus strong feedback could perhaps be inferred by observing two widely separated periods with large gradients.

## 8 DISCUSSION

In this paper, we have described the basic mechanisms relevant to computing the globally-averaged 21 cm signal from high redshifts. The basic structure of the background depends on three crucial transition points: when  $T_S \rightarrow T_K$  (due to the Wouthuysen-Field effect), when  $T_K$  first exceeds  $T_\gamma$  (most likely due to X-ray heating, possibly together with weak shocks), and reionization. The relative timing of these three transitions determines how much we can learn from the 21 cm transition.

We have examined the range of possible signals and empha-

sized their qualitative features. If Pop II stars dominate the background, and if their X-ray emission (per unit star formation rate) is comparable to that in the local Universe ( $f_X \approx 1$ ), Ly $\alpha$  coupling will become efficient before X-ray heating. This leads to a relatively strong absorption epoch (with a peak  $|\delta T_b| \sim 100$  mK) until X-rays cause  $T_K \gg T_\gamma$ . Once that occurs,  $\delta T_b$  saturates until reionization begins – which is well after the heating transition so long as  $f_X \gtrsim 1$ . Such histories contain long periods in which density fluctuations dominate the 21 cm signal, which is useful for studying cosmological parameters (Bowman et al. 2005; McQuinn et al. 2005). This points to an important benefit of our calculation: it provides a basis for evaluating the expected amplitude of the 21 cm *fluctuations* during various phases of structure formation. Cosmological measurements, spin temperature fluctuations (Barkana & Loeb 2005b; Pritchard & Furlanetto 2005), minihalos (Iliev et al. 2002; Furlanetto & Oh 2006), and reionization itself must all be placed in their proper contexts, and this is a first step in that direction.

If very massive Pop III stars dominate reionization, we expect a rather different history.<sup>9</sup> Because these stars are so hot, the number of Ly $\alpha$  photons per ionizing photon is much smaller. Thus the Ly $\alpha$  coupling transition occurs much nearer to reionization, although the reionization epoch will still be visible in the 21 cm transition. With these stellar populations, disentangling the effects of  $T_S$  and  $\bar{x}_i$  may be more difficult. It would be even more complicated if the X-ray heating transition also occurs during reionization (which it could if we calibrate to the local X-ray luminosity-star formation rate relationship). On the other hand, they could easily have much larger X-ray luminosities, perhaps eliminating the absorption epoch altogether.

A substantial quasar population (seeded by the remnants of massive Pop III stars, for example) could also eliminate the absorption epoch, because such objects have large X-ray luminosities. We have conservatively ignored this possibility because the known population of bright quasars contributes little to reionization (Fan et al. 2004) and does not affect the thermal history significantly (Venkatesan et al. 2001), but this is not to say that “miniquasars” will be unimportant (Oh 2001; Glover & Brand 2003; Madau et al. 2004; Kuhlen & Madau 2005) – although they are unlikely to dominate the ionizing photon budget (Dijkstra et al. 2004; Salvaterra et al. 2005). These sources would only affect our predictions before X-ray heating from stars becomes significant – thus observing the absorption epoch (or lack thereof) could help to constrain their significance. At lower redshifts, and especially during reionization, miniquasars are unimportant for the 21 cm background because stars easily suffice to heat the IGM above  $T_\gamma$ .

Another uncertainty is our simple model for shock heating (Furlanetto & Loeb 2004). While it appears to provide a reasonable description of shocks produced as part of the cosmic web (Kuhlen et al. 2006), some simulations may imply that the low-density IGM could also host weak shocks (Gnedin & Shaver 2004). These are not included in the model and deserve further study. As with quasars, these would not affect our predictions during reionization, but they could shorten or even eliminate the absorption epoch.

Clearly, measuring the mean  $\delta T_b(z)$  would offer insight into the earliest generation of luminous sources (Madau et al. 1997; Shaver et al. 1999; Tozzi et al. 2000; Gnedin & Shaver 2004). How

<sup>9</sup> If metal-free stars have a more or less normal Salpeter IMF, they produce histories resembling those of our Pop II models.

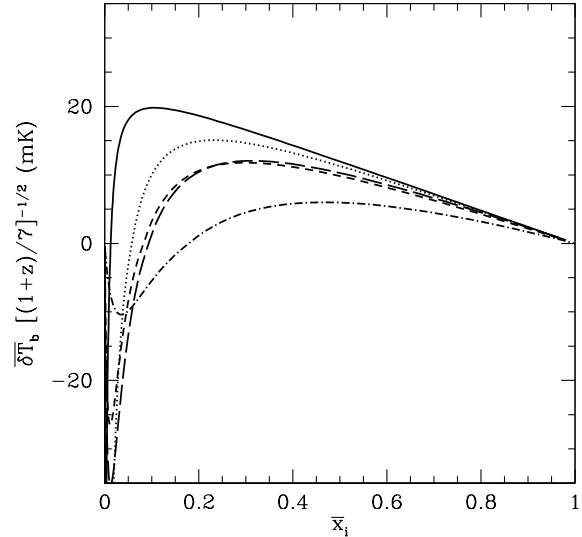


**Figure 4.** Brightness temperature as a function of  $\bar{x}_i$  in several different scenarios. We have removed the redshift dependence of the underlying signal for clarity. The solid and short-dashed curves show our fiducial Pop II and Pop III cases, respectively. The dotted curve uses sets  $f_X = 0.2$  for Pop II stars, and the dot-dashed curve uses  $f_{esc} = 1$  and  $f_X = 0.5$  for Pop III stars. Finally, the long-dashed curve corresponds to the solid curve in Fig. 3.

useful might these measurements be for quantitative constraints? Sethi (2005) computed the sky-averaged 21 cm signal, including Ly $\alpha$  coupling, X-ray heating, and ionization in a restricted range of models (including non-uniform X-ray heating but ignoring Ly $n$  photons, Pop III stars, and feedback, for example). The qualitative features are similar to our Pop II models, although we predict a much wider range of possibilities given the uncertainties in the models.

Treating the efficiency of each process as a free parameter, Sethi (2005) considered how well these parameters could be measured from  $\delta T_b(z)$ . Because (with Pop II stars) heating generally occurs well before reionization, he found that  $\bar{x}_i(z)$  could be well-constrained. We find considerably larger degeneracies. Figure 4 shows the brightness temperature as a function of  $\bar{x}_i$ , with the expected redshift dependence of  $\delta T_b$  in a fully neutral universe removed. We show several different scenarios with a wide range of ionizing and X-ray heating efficiencies. To determine  $\bar{x}_i$  precisely, we would hope that all these curves would overlap. Indeed they do approach each other for  $\bar{x}_i \gtrsim 0.5$ , but earlier in reionization the histories differ substantially. In most cases, the  $(1 - T_S/T_\gamma)$  factor has not yet saturated in this regime, either because of delayed Ly $\alpha$  coupling (usually the case for Pop III stars) or relatively late X-ray heating (particularly in the dotted curve). Thus we predict that, in the absence of other constraints,  $\bar{x}_i$  cannot be determined with certainty from the 21 cm background alone unless it is large.

The most straightforward observation would be to measure  $\delta T_b(z)$  directly. Because this is an all-sky signal, single-dish measurements (even with a modest-sized telescope) can easily reach the required mK sensitivity. However, the much stronger synchrotron foregrounds (primarily from the Galaxy; see Furlanetto et al. 2006 for a review) nevertheless make such observations extremely diffi-

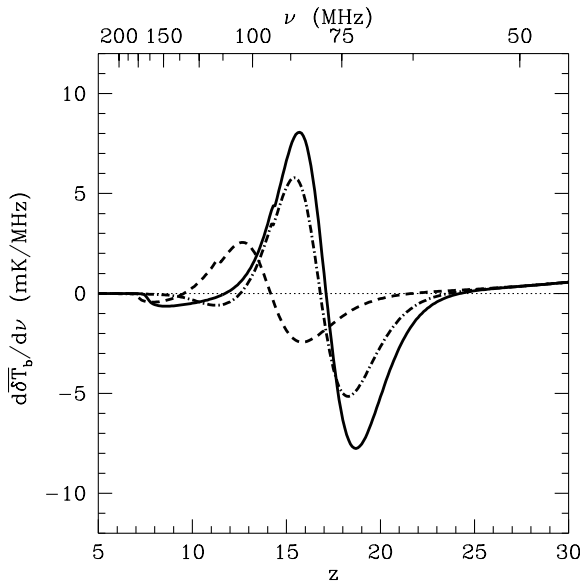


**Figure 5.** Gradient in the cosmological 21 cm signal for several models: our fiducial Pop II history (solid curve), our fiducial Pop III history (dashed curve), and a history with strong feedback (dot-dashed curve, corresponding to the solid curve in Fig. 3). The small hitches in each curve occur at  $T_S \approx T_\gamma$ .

cult. As a rule of thumb, a “quiet” portion of the sky has a brightness temperature

$$T_{\text{sky}} \sim 180 \left( \frac{\nu}{180 \text{ MHz}} \right)^{-2.6} \text{ K.} \quad (25)$$

Clearly, the amplitude of the cosmological signal will be impossible to extract from the foregrounds. But the spectral structure of the 21 cm background imprints features on the (otherwise smooth) spectrum that may be separable. Figure 5 shows the expected gradients in a few of our models. During reionization, we typically have  $d\delta T_b/dz \lesssim 1 \text{ mK MHz}^{-1}$ , over three orders of magnitude smaller than the foregrounds. Without feedback, the gradients tend to increase throughout reionization; with feedback, they peak earlier on. The gradients can be much larger during the absorption era, partly because the signal can vary over a much wider range and partly because  $d\nu/dz$  also decreases. Of course, the foreground gradients also increase significantly at these low frequencies (by about an order of magnitude at  $\nu \approx 90 \text{ MHz}$  according to eq. 25), so it is not clear which regime will actually be easier to constrain. Separating the cosmological signal promises to be a challenge (Shaver et al. 1999; Gnedin & Shaver 2004) and will be easier in histories with strong features (in which feedback does not slow reionization, for example).

The limiting factors in direct measurements are likely to be systematics (Shaver et al. 1999). Foregrounds vary across the sky, which couples to the frequency dependent beam and sidelobes (though the variation should be smooth and hence removable; Oh & Mack 2003). One strategy to avoid confusion with features in the foreground is to use multiple (wide) fields, in which foregrounds are presumably uncorrelated but across which the cosmological signal would be constant. Hydrogen recombination lines leave spectral features throughout the relevant frequency range, but they can be removed through follow-up observations with high spectral resolution. Finally, the biggest challenge will be calibrat-

ing the telescope response to better than one part in  $10^5$  over a wide frequency range. Internal loads of sufficient quality may be difficult to find.

Fortunately, even if systematics do prove to be insurmountable, there are other ways to extract the mean signal. Cooray (2005) pointed out that scattering by a massive, low-redshift galaxy cluster can shift the spectrum in frequency space, so that differential measurements between the cluster and background may reveal the global spectrum. This avoids many systematics, but given the relatively small angular size of clusters may not measure the truly “global” signal. A second possibility is to use the 21 cm fluctuation amplitude to measure the mean background, provided three-dimensional anisotropies can be measured (Barkana & Loeb 2005a). For example, McQuinn et al. (2005) showed that, when density (and velocity) fluctuations dominate the signal, the overall signal amplitude can be extracted by combining 21 cm data with CMB data. (They phrased their constraint as  $\bar{x}_i$ , but in more general models it corresponds to the mean brightness temperature.)

Despite these difficulties, the global 21 cm background would be an extremely useful tool in understanding the overall evolution of the first sources of light. Together with the fluctuating signal (see Furlanetto et al. 2006 and references therein), the global background could reveal many of the important properties of the “twilight zone” of structure formation.

I thank S. P. Oh for insightful comments on the manuscript, A. Loeb and J. Pritchard for helpful discussions, and R. Barkana for sharing the stellar spectra used in §4. I also thank the Tapir group at Caltech for hospitality while some of this work was completed.

## REFERENCES

- Barkana R., Loeb A., 2001, *Physics Reports* , 349, 125  
 Barkana R., Loeb A., 2005a, *ApJ* , 624, L65  
 Barkana R., Loeb A., 2005b, *ApJ* , 626, 1  
 Bharadwaj S., Ali S. S., 2004, *MNRAS* , 352, 142  
 Bouwens R. J., et al., 2004, *ApJ* , 616, L79  
 Bowman J. D., Morales M. F., Hewitt J. N., 2005, submitted to *ApJ* (astro-ph/0512262)  
 Bromm V., Kudritzki R. P., Loeb A., 2001, *ApJ* , 552, 464  
 Cen R., 2003a, *ApJ* , 591, L5  
 Cen R., 2003b, *ApJ* , 591, L2  
 Cen R., 2006, submitted to *ApJ* (astro-ph/0601010)  
 Cen R., Ostriker J. P., 1999, *ApJ* , 514, 1  
 Chen X., Miralda-Escudé J., 2004, *ApJ* , 602, 1  
 Choudhury T. R., Ferrara A., 2005, *MNRAS* , 361, 577  
 Ciardi B., Ferrara A., 2005, *Space Science Reviews*, 116, 625  
 Ciardi B., Madau P., 2003, *ApJ* , 596, 1  
 Ciardi B., Scannapieco E., Stoehr F., Ferrara A., Iliev I. T., Shapiro P. R., 2005, *MNRAS* , in press (astro-ph/0511623)  
 Ciardi B., Stoehr F., White S. D. M., 2003, *MNRAS* , 343, 1101  
 Cooray A., 2005, submitted to *MNRAS* (astro-ph/0511240)  
 Davé R., et al., 2001, *ApJ* , 552, 473  
 Dijkstra M., Haiman Z., Loeb A., 2004, *ApJ* , 613, 646  
 Dijkstra M., Haiman Z., Rees M. J., Weinberg D. H., 2004, *ApJ* , 601, 666  
 Efstathiou G., 1992, *MNRAS* , 256, 43  
 Fan X., et al., 2001, *AJ* , 122, 2833  
 Fan X., et al., 2004, *AJ* , 128, 515  
 Fan X., et al., 2005, in press at *AJ* (astro-ph/0512080)  
 Field G. B., 1958, *Proc. I.R.E.*, 46, 240  
 Field G. B., 1959, *ApJ* , 129, 536  
 Fukugita M., Kawasaki M., 2003, *MNRAS* , 343, L25  
 Furlanetto S. R., Loeb A., 2004, *ApJ* , 611, 642  
 Furlanetto S. R., Loeb A., 2005, *ApJ* , 634, 1  
 Furlanetto S. R., McQuinn M., Hernquist L., 2006, *MNRAS* , 365, 115

- Furlanetto S. R., Oh S. P., 2005, *MNRAS* , 363, 1031
- Furlanetto S. R., Oh S. P., 2006, in preparation
- Furlanetto S. R., Oh S. P., Briggs F. H., 2006, *Physics Reports*, in preparation
- Gilfanov M., Grimm H.-J., Sunyaev R., 2004, *MNRAS* , 347, L57
- Glover S. C. O., Brand P. W. J. L., 2003, *MNRAS* , 340, 210
- Gnedin N. Y., Hui L., 1998, *MNRAS* , 296, 44
- Gnedin N. Y., Shaver P. A., 2004, *ApJ* , 608, 611
- Grimm H.-J., Gilfanov M., Sunyaev R., 2003, *MNRAS* , 339, 793
- Haiman Z., 2004, in *Coevolution of Black Holes and Galaxies The First Nonlinear Structures and the Reionization History of the Universe*. p. 67
- Haiman Z., Holder G. P., 2003, *ApJ* , 595, 1
- Heger A., Woosley S. E., 2002, *ApJ* , 567, 532
- Hirata C. M., 2005, submitted to *MNRAS* (astro-ph/0507102)
- Hogan C. J., Rees M. J., 1979, *MNRAS* , 188, 791
- Iliev I. T., Scannapieco E., Shapiro P. R., 2005, *ApJ* , 624, 491
- Iliev I. T., Shapiro P. R., Ferrara A., Martel H., 2002, *ApJ* , 572, L123
- Kang H., Ryu D., Cen R., Song D., 2005, *ApJ* , 620, 21
- Kitayama T., Ikeuchi S., 2000, *ApJ* , 529, 615
- Koyama K., Petre R., Gotthelf E. V., Hwang U., Matsuura M., Ozaki M., Holt S. S., 1995, *Nature* , 378, 255
- Kuhlen M., Madau P., 2005, *MNRAS* , 363, 1069
- Kuhlen M., Madau P., Montgomery R., 2006, *ApJ* , 637, L1
- Leitherer C., et al., 1999, *ApJS* , 123, 3
- Lidz A., Oh S. P., Furlanetto S. R., 2006, *ApJ* , 639, L47
- Liszt H., 2001, *A&A* , 371, 698
- Madau P., Meiksin A., Rees M. J., 1997, *ApJ* , 475, 429
- Madau P., Rees M. J., Volonteri M., Haardt F., Oh S. P., 2004, *ApJ* , 604, 484
- McQuinn M., Zahn O., Zaldarriaga M., Hernquist L., Furlanetto S. R., 2005, submitted to *ApJ* (astro-ph/0512263)
- Mesinger A., Haiman Z., 2004, *ApJ* , 611, L69
- Miniati F., Ryu D., Kang H., Jones T. W., Cen R., Ostriker J. P., 2000, *ApJ* , 542, 608
- Miralda-Escudé J., Haehnelt M., Rees M. J., 2000, *ApJ* , 530, 1
- Nath B. B., Silk J., 2001, *MNRAS* , 327, L5
- Nusser A., 2005, *MNRAS* , 359, 183
- Oh S. P., 2001, *ApJ* , 553, 499
- Oh S. P., Mack K. J., 2003, *MNRAS* , 346, 871
- Onken C. A., Miralda-Escudé J., 2004, *ApJ* , 610, 1
- Page L., et al., 2006, submitted to *ApJ* (astro-ph/0603450)
- Peebles P. J. E., 1993, *Principles of Physical Cosmology*. Princeton: Princeton University Press
- Press W. H., Schechter P., 1974, *ApJ* , 187, 425
- Pritchard J. R., Furlanetto S. R., 2005, submitted to *MNRAS* (astro-ph/0508381)
- Ranalli P., Comastri A., Setti G., 2003, *A&A* , 399, 39
- Rees M. J., 1986, *MNRAS* , 222, 27
- Rephaeli Y., Gruber D., Persic M., 1995, *A&A* , 300, 91
- Ricotti M., Ostriker J. P., Gnedin N. Y., 2005, *MNRAS* , 357, 207
- Rybicki G. B., 2006, submitted to *ApJ* (astro-ph/0603047)
- Salvaterra R., Haardt F., Ferrara A., 2005, *MNRAS* , 362, L50
- Schaerer D., 2002, *A&A* , 382, 28
- Scott D., Rees M. J., 1990, *MNRAS* , 247, 510
- Seager S., Sasselov D. D., Scott D., 2000, *ApJS* , 128, 407
- Sethi S. K., 2005, *MNRAS* , p. 812
- Shapiro P. R., Ahn K., Alvarez M. A., Iliev I. T., Martel H., Ryu D., 2005, submitted to *ApJ* (astro-ph/0512516)
- Shaver P. A., Windhorst R. A., Madau P., de Bruyn A. G., 1999, *A&A* , 345, 380
- Shull J. M., van Steenberg M. E., 1985, *ApJ* , 298, 268
- Smith F. J., 1966, *Plan. Space Sci.*, 14, 929
- Somerville R. S., Livio M., 2003, *ApJ* , 593, 611
- Spergel D. N., et al., 2006, submitted to *ApJ* (astro-ph/0603449)
- Sunyaev R. A., Zeldovich Y. B., 1972, *A&A* , 20, 189
- Thoul A. A., Weinberg D. H., 1996, *ApJ* , 465, 608
- Tozzi P., Madau P., Meiksin A., Rees M. J., 2000, *ApJ* , 528, 597
- Valageas P., Schaeffer R., Silk J., 2002, *A&A* , 388, 741
- Venkatesan A., Giroux M. L., Shull J. M., 2001, *ApJ* , 563, 1
- Whalen D., Abel T., Norman M. L., 2004, *ApJ* , 610, 14
- Wouthuysen S. A., 1952, *AJ* , 57, 31
- Wyithe J. S. B., Loeb A., 2003a, *ApJ* , 586, 693
- Wyithe J. S. B., Loeb A., 2003b, *ApJ* , 588, L69
- Wyithe J. S. B., Loeb A., 2004, *Nature* , 427, 815
- Wyithe J. S. B., Loeb A., Carilli C., 2005, *ApJ* , 628, 575
- Wyithe S., Loeb A., 2005, submitted to *ApJ* (astro-ph/0508604)
- Zaldarriaga M., Furlanetto S. R., Hernquist L., 2004, *ApJ* , 608, 622
- Zygelman B., 2005, *ApJ* , 622, 1356